

New data on $\vec{\gamma}\vec{p} \rightarrow \eta p$ with polarized photons and protons and their implications for $N^* \rightarrow N\eta$ decays

J. Müller^a, J. Hartmann^a, M. Grüner^a, F. Afzal^a, A.V. Anisovich^{a,b}, B. Bantes^c, D. Bayadilov^{a,b}, R. Beck^a, M. Becker^a, Y. Beloglazov^b, M. Berlin^d, M. Bichow^d, S. Böse^a, K.-T. Brinkmann^{a,e}, T. Challand^f, V. Crede^g, F. Dietz^e, M. Dieterle^f, P. Drexler^e, H. Dutz^c, H. Eberhardt^c, D. Elsner^c, R. Ewald^c, K. Fernet-Ponse^c, S. Friedrich^e, F. Frommberger^c, C. Funke^a, M. Gottschall^a, A. Gridnev^b, S. Goertz^c, E. Gutz^{a,e}, C. Hammann^a, V. Hannen^e, J. Hannappel^c, J. Herick^d, W. Hillert^c, P. Hoffmeister^a, C. Honisch^a, O. Jahn^c, T. Jude^c, I. Jaegle^f, A. Käser^f, D. Kaiser^a, H. Kalinowsky^a, F. Kalischewski^a, S. Kammer^c, I. Keshelashvili^f, P. Klassen^a, V. Kleber^c, F. Klein^c, E. Klempt^a, K. Koop^a, B. Krusche^f, M. Kube^a, M. Lang^a, I. Lopatin^b, Y. Maghrbi^f, P. Mahlberg^a, K. Makonyi^e, F. Messi^c, V. Metag^e, W. Meyer^d, J. Müllers^a, M. Nanova^e, V. Nikonov^{a,b}, D. Novinski^b, R. Novotny^e, D. Piontek^a, G. Reicherz^d, C. Rosenbaum^a, T. Rostomyan^f, B. Roth^d, A. Sarantsev^{a,b}, C. Schmidt^a, H. Schmieden^c, R. Schmitz^a, T. Seifen^a, V. Sokhoyan^a, A. Thiel^a, U. Thoma^{a,*}, M. Urban^a, H. van Pee^a, D. Walther^a, C. Wendel^a, U. Wiedner^d, A. Wilson^{a,g}, A. Winnebeck^a, L. Witthauer^f,

CBELSA/TAPS Collaboration

^aHelmholtz-Institut für Strahlen- und Kernphysik, Universität Bonn, Germany

^bNational Research Centre "Kurchatov Institute", Petersburg Nuclear Physics Institute, Gatchina, Russia

^cPhysikalisches Institut, Universität Bonn, Germany

^dInstitut für Experimentalphysik I, Ruhr-Universität Bochum, Germany

^eII. Physikalisches Institut, Universität Gießen, Germany

^fPhysikalisches Institut, Universität Basel, Switzerland

^gDepartment of Physics, Florida State University, Tallahassee, FL 32306, USA

Abstract

The polarization observables T, E, P, H , and G in photoproduction of η mesons off protons are measured for photon energies from threshold to $W = 2400$ MeV (T), 2280 MeV (E), 1620 MeV (P, H), or 1820 MeV (G), covering nearly the full solid angle. The data are compared to predictions from the SAID, MAID, JüBo, and BnGa partial-wave analyses. A refit within the BnGa approach including further data yields precise branching ratios for the $N\eta$ decay of nucleon resonances. A $N\eta$ -branching ratio of 0.33 ± 0.04 for $N(1650)1/2^-$ is found, which reduces the large and controversially discussed $N\eta$ -branching ratio difference of the two lowest mass $J^P = 1/2^-$ -resonances significantly.

Keywords: baryon spectroscopy, meson photoproduction, polarization observables

1. Introduction

The properties of excited states of protons and neutrons, their masses, widths and decays, reflect their internal dynamics. Quark models describe the excitation spectrum of nucleons by the interaction of three constituent quarks in a confinement potential adding a residual interaction such as one-gluon [1, 2] or pseudoscalar-meson [3] exchange, or instanton induced interactions [4]. QCD calculations on the lattice [5] – even though using unphysically large quark masses – yield a similar pattern. A very different view assumes that quarks and gluons are not the appropriate degrees of freedom to describe nucleon resonances; instead, resonances are generated dynamically from their hadronic decay products [6, 7, 8, 9]. Properties

of baryon resonances differentiating between the models are of particular importance.

The surprising decay pattern of the two lowest-mass nucleon excitations, $N(1535)1/2^-$ and $N(1650)1/2^-$ with spin-parity $J^P=1/2^-$ and carrying an orbital angular momentum $L=1$, has always been a challenge for model builders. In 2010, the $N\eta$ branching ratio of $N(1535)1/2^-$ was estimated by the Particle Data Group [10] to 45–60%, and only 3–10% for $N(1650)1/2^-$. Several interpretations have been offered to explain the unexpectedly large $N(1535)1/2^- \rightarrow N\eta$ branching ratio:

i) Within the quark model [1], the one-gluon exchange interaction leads to a mixing angle of the two states with defined total quark spin S , $|J=1/2; L=1, S=1/2\rangle$ and $|J=1/2; L=1, S=3/2\rangle$. At this mixing angle, the higher-mass state $N(1650)1/2^-$ nearly decouples from $N\eta$; the lower-mass state $N(1535)1/2^-$ acquires a large $N\eta$ branching ratio.

*Corresponding author.

Email address: thoma@hiskp.uni-bonn.de (U. Thoma)

ii) In the quark model [11], the large $N\eta$ branching ratio is explained as a consequence of a dynamical clusterization into a quark-diquark configuration.

iii) The low mass of the $N(1440)1/2^+$ Roper resonance and the large $N(1535)1/2^- \rightarrow N\eta$ coupling may both be explained by large pentaquark components in their wave functions [12].

iv) In [9, 13], $N(1535)1/2^-$ is generated dynamically and interpreted as quasi-bound $K\Sigma$ - $K\Lambda$ -state decaying strongly into $N\eta$ via coupled-channel effects.

All models agree on the conclusion – driven by experimental information – that the $N(1535)1/2^- \rightarrow N\eta$ branching ratio is much larger than that for $N(1650)1/2^- \rightarrow N\eta$ decays. These results were, however, derived from rather poor data on $\pi^-p \rightarrow \eta n$ and from differential cross sections and the beam asymmetry for $\gamma p \rightarrow \eta p$. Neither data set fully constrains the amplitudes governing pion- or photo-production of η mesons. Thus, a wide range of results on the $N\eta$ branching ratio was reported in the literature.

Vrana *et al.* [14] fitted data on πN inelastic reactions, with πN , ηN and $\pi\pi N$ as admitted final states. When these three final states were included, $N\eta$ branching ratios for $N(1650)1/2^-$ of 16%, 25%, and 6% were derived using different model assumptions. The last model was considered to be the best one, and a branching ratio $\text{BR} = 0.06 \pm 0.01$ was quoted as final result. The authors pointed out that the data on $\pi^-p \rightarrow \eta n$ is both, limited and of uncertain quality. This statement holds true, of course, for all analyses using those data.

Penner and Mosel performed a coupled-channel analysis of a large number of reactions. The authors gave a branching ratio between 0.004 and 0.051 [15, 16]. Shklyar *et al.* [17] gave a branching of 0.01 ± 0.02 , which we read as < 0.03 .

The Bonn-Gatchina group [18] reported a value of 0.18 ± 0.04 from a study of a large body of pion and photo-induced reactions, a value that superseded an earlier fit [19] to a smaller data sample reporting 0.15 ± 0.06 .

A new η MAID2017-solution [20] including the data [21, 22, 23, 24, 25] finds 0.28 ± 0.11 using an $A_{1/2}$ -value of $+0.045$. MAID2018 reports a branching ratio of 0.19 ± 0.06 , using $A_{1/2} = +0.055$ [26]. Both solutions lead to the same $A_{1/2}\sqrt{\text{BR}(N\eta)}$ for $N(1650)1/2^-$.

Shrestha and Manley [27] performed coupled-channel fits to pion-induced reactions and determined a $N\eta$ branching ratio for $N(1650)1/2^-$ of 0.21 ± 0.02 where the error is of statistical nature. Batinic *et al.* fitted data on the reactions $\pi N \rightarrow \pi N$ and ηN and obtained 0.13 ± 0.05 .

Tryasuchev [28] introduces a quantity ξ defined as

$$\xi_{1/2, 3/2} = \sqrt{\frac{k M_p \text{BR}_\eta}{q M_R \Gamma_R}} \cdot A_{1/2, 3/2} \quad (1)$$

with the proton mass M_p and the resonance mass M_R and width Γ_R . k and q are the decay momenta of photon or η in the center-of-mass system. In a fit to data

on η photoproduction, Tryasuchev finds for $N(1650)1/2^-$ the value $\xi_{1/2} = 0.0975 \text{ GeV}^{-1}$, from which we deduce $A_{1/2} \cdot \sqrt{\text{BR}_\eta} = 0.034 \text{ GeV}^{-1/2}$ (using PDG-values [31] for $M_R \Gamma_R$). No error is given in [28] for ξ . With this value for ξ and our value for $A_{1/2}$ reported below, the $N\eta$ branching ratio should be in the order of 1.

The analysis of η production in pion and photo-induced reactions by the Jülich/Bonn group [32] finds a $N\eta$ branching ratio that is more than a factor six larger for $N(1535)1/2^-$ than for $N(1650)1/2^-$.

In this letter, we present results from a study of $\gamma p \rightarrow \eta p$ using a longitudinally or transversely polarized target with polarization p_T and linearly or circularly polarized photons with polarization p_γ or p_\odot , respectively. The results of these different data sets are presented here in a single letter since we believe that only the complete information can constrain a partial-wave analysis sufficiently well to lead to unambiguous results on $N^* \rightarrow N\eta$ decays. For details on the measurements and data analyses, we quote earlier publications on $\gamma p \rightarrow \pi^0 p$ on E [33, 34], T, P, H [35, 36], and G [37, 38].

2. The experiment

2.1. Experimental setup

The experiment was carried out at the ELectron Stretcher Accelerator ELSA in Bonn [39]. Photons with circular polarization p_\odot were produced by scattering a 2.335 GeV beam of longitudinally polarized electrons off a bremsstrahlung target: p_\odot decreases from 0.63 at the maximal tagged photon energy of 2.29 GeV to 0.34 at 1 GeV. Linearly polarized photons with polarization p_γ stem from coherent bremsstrahlung of 3.2 GeV electrons off an aligned diamond. For the measurement of T, P , and H , the coherent edge of the crystal was set to achieve a maximum polarization of $p_\gamma = 65\%$ at 850 MeV. For G , three polarization settings were used. Here, the maximum linear polarization reached was 65% at 860 MeV, 59% at 1050 MeV, and 55% at 1270 MeV.

The electrons passed through a magnet hitting a tagging hodoscope, which defined the energy of the bremsstrahlung photons. The photon beam impinged on the Bonn frozen spin butanol ($\text{C}_4\text{H}_9\text{OH}$) target containing either longitudinally or transversely polarized protons [40]. The target was surrounded by a three-layer scintillation fiber detector [41] used for the identification of charged particles and by the Crystal Barrel electromagnetic calorimeter [42] consisting of 1230 CsI(Tl)-crystals. In the forward direction below polar angles of 30° , two further calorimeters, the forward detector consisting of 90 CsI(Tl)-crystals and the forward TAPS-wall [43] (216 BaF₂ crystals), provided calorimetric information. Plastic scintillators in front of the forward crystals allowed for the identification of charged particles. A CO₂ Cherenkov detector placed before the forward TAPS-wall vetoed signals due to electron

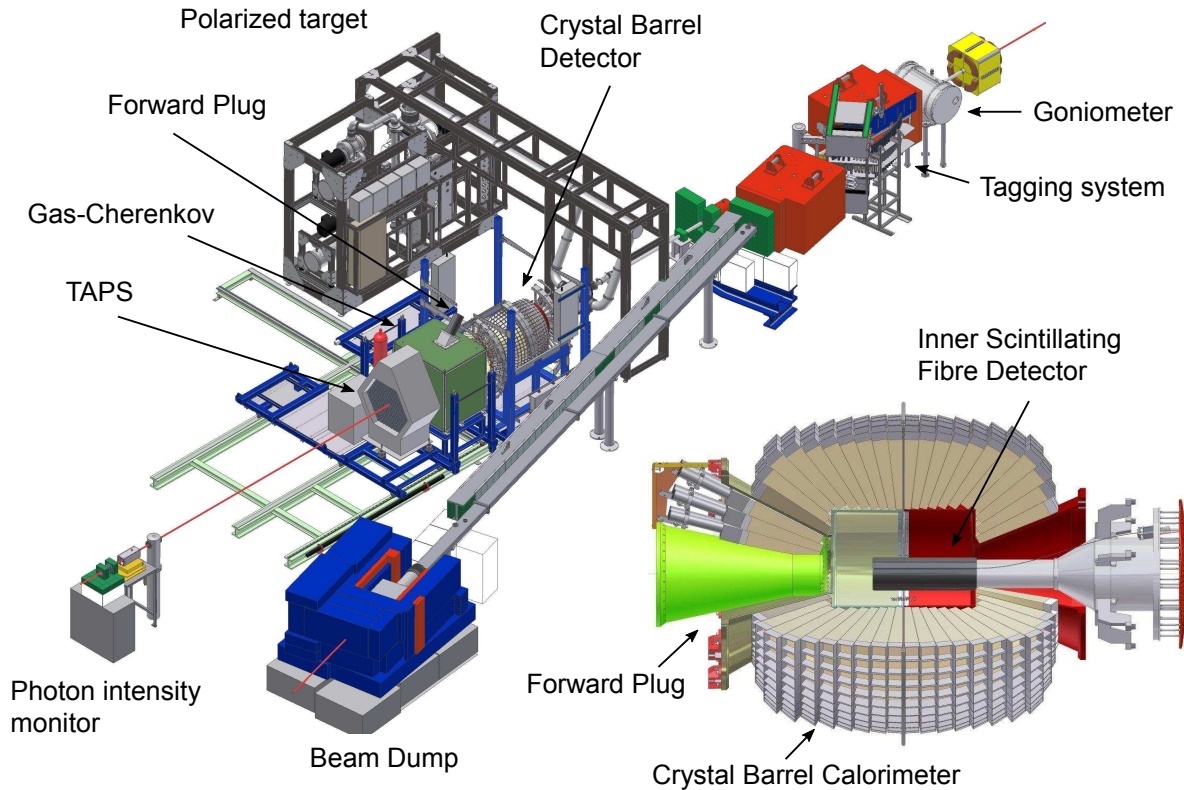


Figure 1: Experimental setup of the CBELSA/TAPS experiment.

or positron hits, which are due to electromagnetic background produced in the target. Figure 1 shows an overview of the experimental setup.

2.2. Reconstruction and event selection

Photon candidates were defined by hits in the calorimeters and no related hit in the scintillation fiber detector or the plastic scintillation counters. The four-momenta of photons were determined by measuring their energies and directions assuming that the photons originated from the target center. Charged particles were identified by hits in one of the scintillation counters associated with a calorimeter hit. In the case of the longitudinally polarized target, the electromagnetic background was considerably lower, and charged particles were also identified by hits in the inner detector only. In the analysis of data with the transversely polarized target, photon and proton candidates were reconstructed from events which had only hits in the calorimeters. Then, the best kinematic combination was chosen with one meson and one proton in the final state.

Events due to $\gamma p \rightarrow \gamma\gamma p$ were selected by choosing events satisfying the following criteria: two photon and one proton candidates had to be detected; the invariant mass of the two photons had to agree within $\pm 2\sigma$ with the η mass (see Fig. 2); the missing mass X from $\gamma p \rightarrow$

$\gamma\gamma X$ had to agree with the proton mass within $\pm 2\sigma$, the azimuthal angle between the direction of proton and η was requested to be 180° within a $\pm 2\sigma$ window (coplanarity), an additional $\pm 2\sigma$ -cut on the respective polar angle was performed for part of the data sets. All these cuts were done taking the energy-dependent width of the respective quantity into account. In addition, a time coincidence was required between the tagger hit and the reaction products, and random time background was subtracted.

2.3. Dilution factor

In a butanol target, polarizable free protons (f) as well as nucleons bound (b) in carbon or oxygen nuclei contribute to the count rate. The contribution of bound nucleons was determined using a carbon foam target within the cryostat with approximately the same density as the carbon and oxygen part of the butanol target. The coplanarity distribution of events produced off bound nucleons is wider than the one for free protons. This effect was used to determine – for each bin in energy and angle – the fraction of the reactions off free protons in the data collected with the butanol target (see Fig. 3). This fraction is called dilution factor

$$d(E_\gamma, \cos\theta_\eta) = N^f / (N^f + N^b)$$

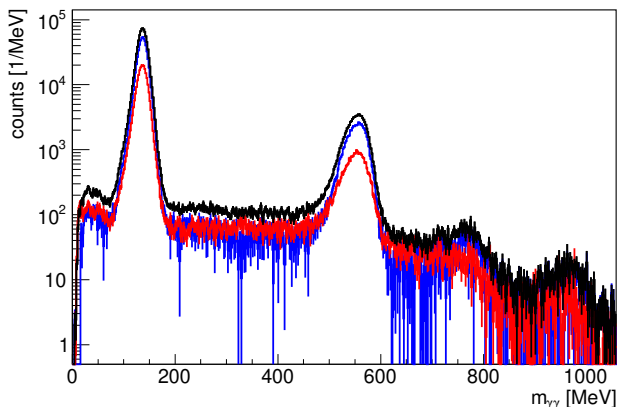


Figure 2: $\gamma\gamma$ -invariant mass distribution for the data with transversally polarized target and linearly polarized photons, black: butanol data, red: carbon data, blue: difference. Random time background already subtracted.

and was determined as $d = (N_{\text{butanol}} - s \cdot N_{\text{carbon}}) / N_{\text{butanol}}$. The carbon normalization factor s was determined by comparing the carbon data to the butanol data, excluding kinematic regions where contributions from free protons can be expected. The dilution factor, as determined for the T, P, H -data, is shown in Fig. 3, further examples are given in [33, 34, 35, 37].

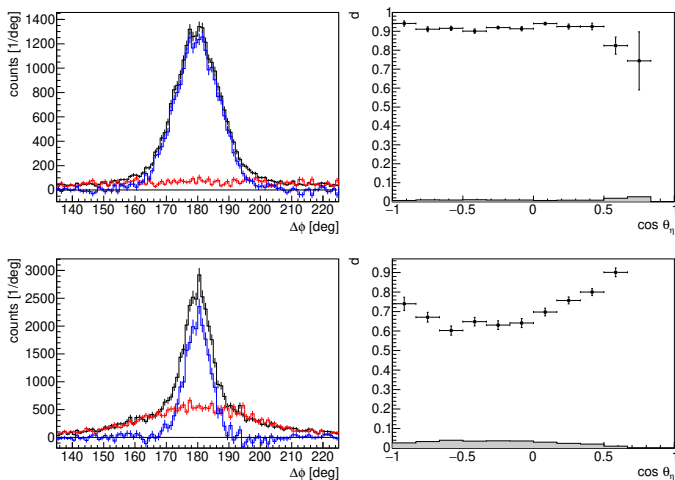


Figure 3: Left: coplanarity spectra (T, P, H -data), black: butanol data, red: scaled carbon data, blue: subtracted spectrum (free protons). Right: Dilution factor d . Upper row: $1513 \text{ MeV} < W < 1531 \text{ MeV}$, lower row: $1660 \text{ MeV} < W < 1716 \text{ MeV}$. The gray bands show the systematic uncertainty due to normalization of carbon data.

2.4. Polarization observables

The helicity asymmetry E requires circularly polarized photons and longitudinally polarized protons. It can be determined as

$$E = \frac{N_{1/2} - N_{3/2}}{N_{1/2} + N_{3/2}} \cdot \frac{1}{d} \cdot \frac{1}{p_{\odot} p_T}, \quad (2)$$

where $N_{1/2}$ and $N_{3/2}$ are the number of events observed with photon and target polarization in opposite or paral-

lel directions, normalized to the corresponding number of incident photons.

G can be deduced from the correlation between the photon polarization plane and the scattering plane for protons polarized along the direction of the incoming photon. The number of events N as a function of the azimuthal angle ϕ between the two planes is given by

$$\frac{N(\phi)}{N_0} = 1 - p_{\gamma} \cdot [\Sigma_{\text{eff}} \cos(2\phi) - d p_T G \sin(2\phi)], \quad (3)$$

where N_0 is given by averaging $N(\phi)$ over ϕ . Σ_{eff} mixes the beam asymmetry of free and bound nucleons.

The observables T, P , and H can be measured simultaneously when a transversely polarized target and a linearly polarized photon beam are used. In that case, the azimuthal distribution of events is given by

$$\begin{aligned} \frac{N(\phi)}{N_0} = & 1 - p_{\gamma} \Sigma_{\text{eff}} \cos(2\phi) + d p_T T \sin(\phi - \alpha) \\ & - d p_T p_{\gamma} P \cos(2\phi) \sin(\phi - \alpha) \\ & + d p_T p_{\gamma} H \sin(2\phi) \cos(\phi - \alpha), \end{aligned} \quad (4)$$

where α is the azimuthal angle between the target polarization vector and the photon polarization plane. T, P , and H are determined, for each $(E_{\gamma}, \cos \theta_{\eta})$ bin, from an event-based maximum likelihood fit [44] to the measured azimuthal distribution of events.

2.5. Systematic Uncertainties

The data-taking periods, the target and beam polarization as well as the analyses methods used to extract the different observables were not identical for the data presented here; therefore the systematic uncertainties for the different data sets are discussed separately in the following. The systematic uncertainties of all observables include contributions from possible background events, the determination of the dilution factor, and the polarization degrees of target (all observables) and beam (only E, G, H, P).

The polarization of the circularly polarized photon beam was calculated using the polarization transfer from the longitudinally polarized incident electron beam [45]. The electron polarization was measured in parallel to data-taking using a Møller polarimeter with a relative systematic uncertainty of 3.3% [34]. The polarization of the linearly polarized photon beam was determined from the measured photon intensity spectrum using a software [46] based on the analytic bremsstrahlung (ANB) calculation [47]. For the measurement of G the relative uncertainty was 5%. For the observables P and H , measured only up to $E_{\gamma} = 933 \text{ MeV}$, a relative uncertainty of 4% was achieved.

The polarization of the dynamically polarized target protons was measured using an NMR system [48]. It was calibrated using the proton polarization in thermal equilibrium. A relative systematic uncertainty of 2% was reached for all data sets.

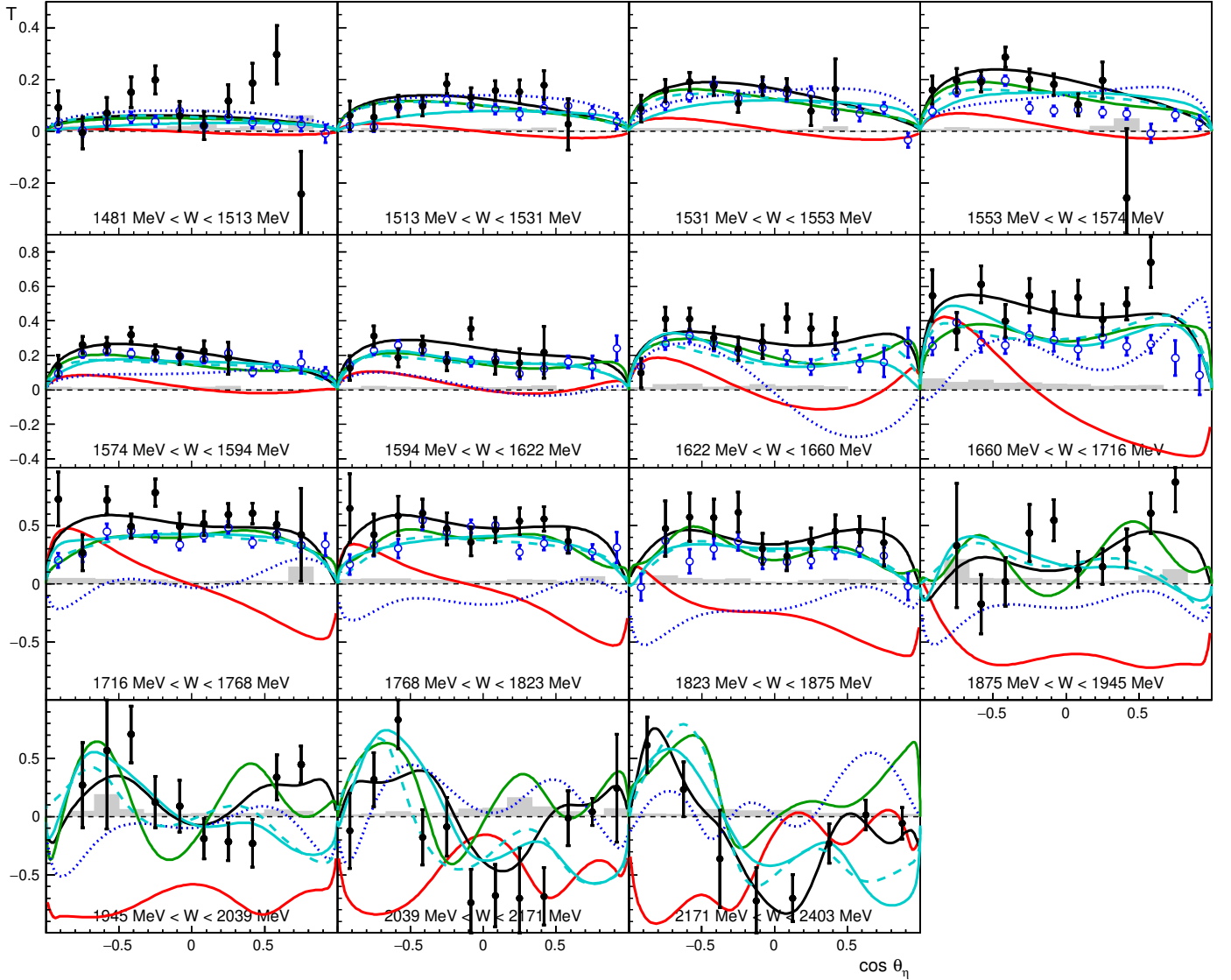


Figure 4: The polarization observable T as function of $\cos\theta_\eta$, where θ_η is the η production angle in the cms for different cms energy ranges. The curves represent different models. Black: BnGa refit; red: BnGa2011-02 [18]; green: MAID2018 [26]; dark blue (dotted): SAID (GE09) [51]; light blue: JüBo 2015 [32] (dashed) and JüBo 2015-3 [22] (solid). The different PWA curves are calculated at the central energy of each bin. (JüBo 2015-3, included the recent CLAS-data on E [22], MAID2018 [26] in addition to E from CLAS [22], also T and F from MAMI [21].) The systematic errors due to photon and proton polarization, dilution factor, and background contamination are shown as a gray band. Recent data from MAMI [21] are shown for comparison as blue open points (due to different binning, the energies differ by up to $\Delta W = 14$ MeV).

The determination of the dilution factor d relies on the relative normalization of the carbon data. A conservative uncertainty of 10% was assumed for the normalization factor s . Close to threshold, where $d > 0.9$, this yields a systematic uncertainty $\Delta d < 0.01$. Since d decreases with energy, its uncertainty increases up to $\Delta d = 0.05$ for $E_\gamma > 2$ GeV. A systematic uncertainty of comparable magnitude was determined for the observable G using a different method. Here either carbon or carbon and LH₂-data were used in combination with the butanol data to determine d . The resulting differences were considered as systematic uncertainties.

Background contamination of the event samples was found to be below 2% in most bins. Only a few bins at the

edge of the detector acceptance exhibit more background, up to 5%–15%, depending on the data set and exact selection criteria used. For the observable E the background was found to be unpolarized, and the values of E were corrected accordingly. For the other observables, the asymmetry of the background could not be constrained significantly because of the limited size of the event samples and the small background contribution. Instead, the relative background contamination was taken as an additional systematic uncertainty of the observables.

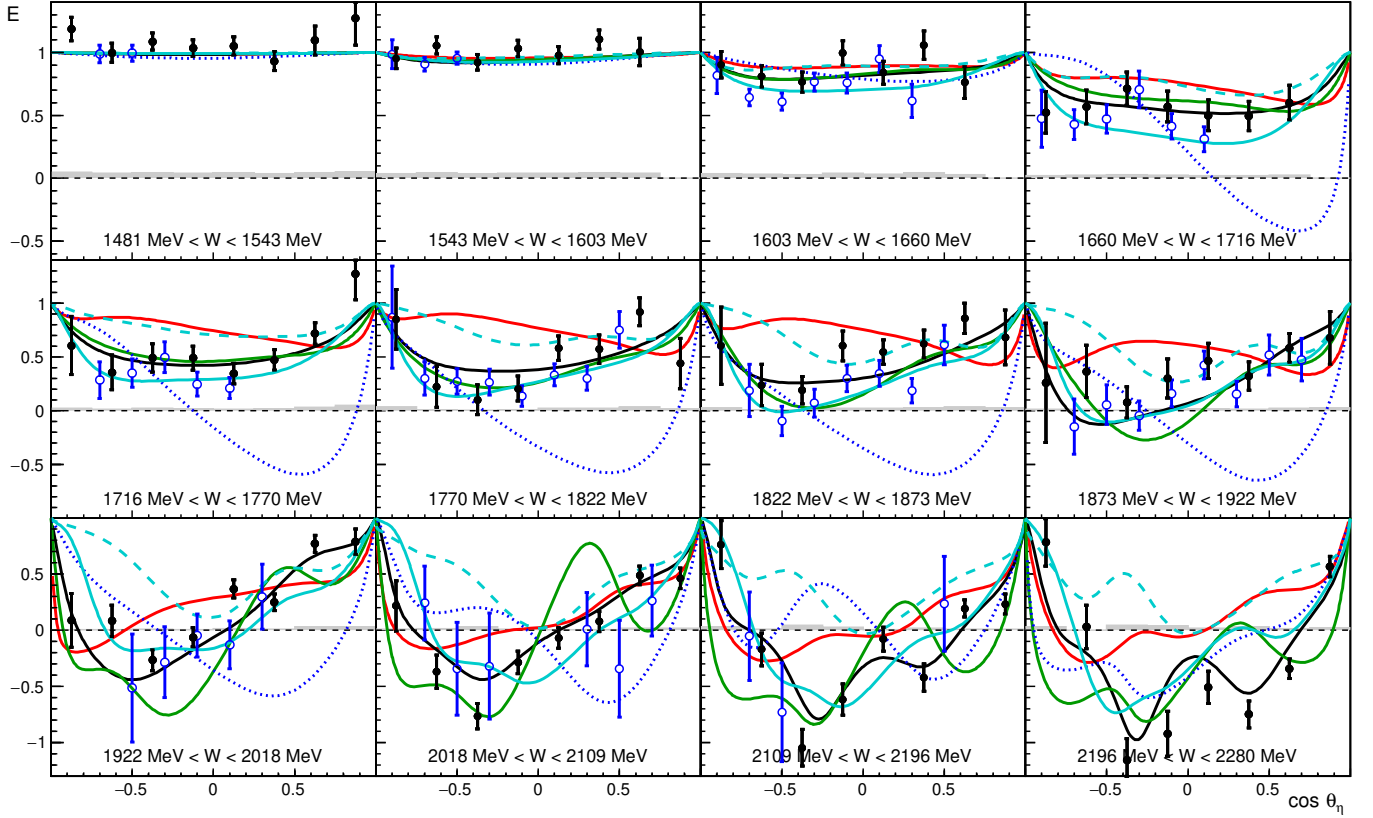


Figure 5: The double polarization observable E as function of $\cos\theta_\eta$, where θ_η is the η production angle in the cms for different cms energy ranges. See caption of Fig. 4 for an explanation of the symbols. Recent data from CLAS [22] are shown for comparison as blue open points (due to different binning, the energies differ by up to half of the bin size).

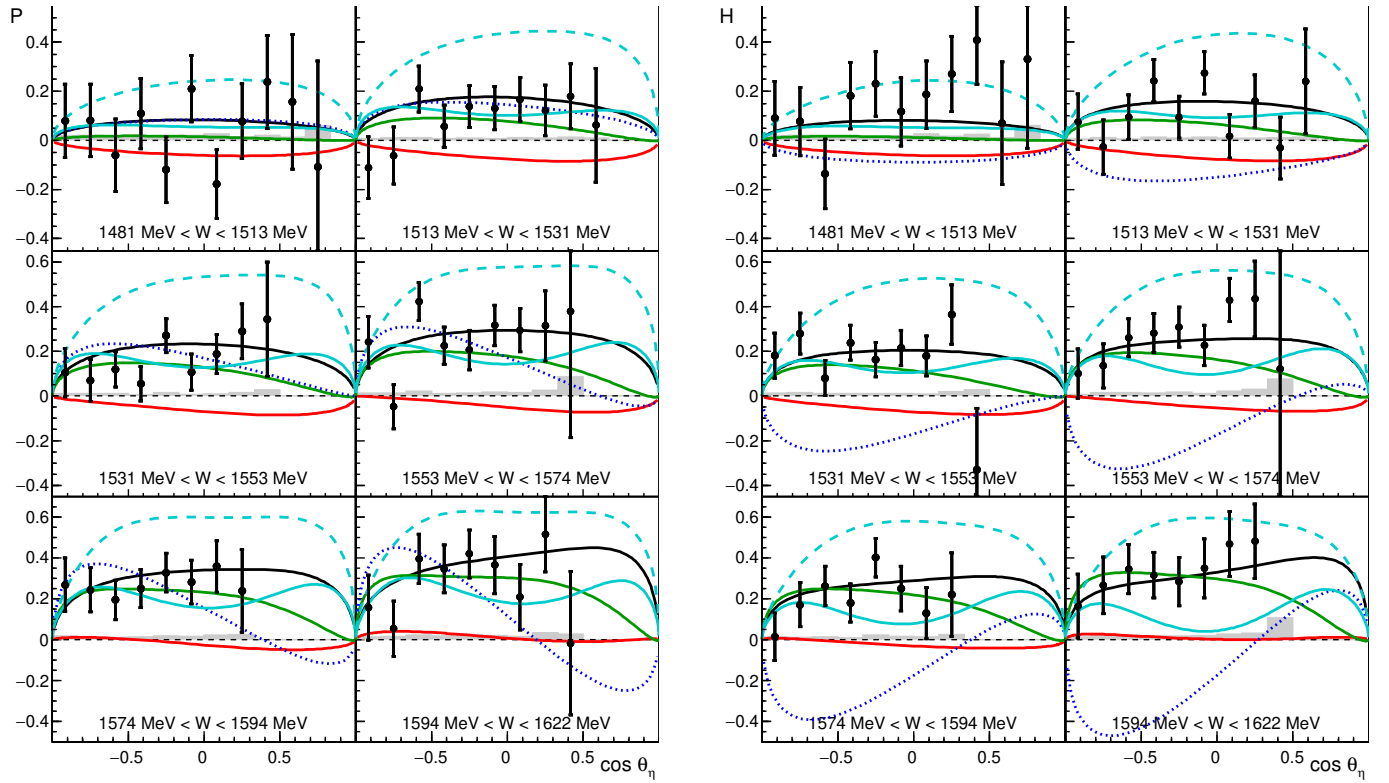


Figure 6: The double polarization observables P and H as functions of $\cos\theta_\eta$, where θ_η is the η production angle in the cms for different cms energy ranges. See caption of Fig. 4 for an explanation of the symbols.

3. Results

3.1. Observables

Figures 4–7 show the resulting double polarization observables T , E , P , H , and G . Only for E and T , earlier data exist that cover more than a few energy and angular bins. CLAS has published data on E [22]. Our data extend the energy and angular range of the CLAS data. Within uncertainties, the CLAS data are in good agreement with our findings (see Fig. 5).

In the low-energy region, E is expected to be close to +1, since this region is dominated by one single resonance with spin-parity $J^P = 1/2^-$. The asymmetry should not exceed one. As visible in Fig. 5, three of the data points in the first energy bin exceed one beyond their statistical 1σ error. Averaging all data points in the first energy bin yields $E = 1.05 \pm 0.03_{\text{stat}} \pm 0.04_{\text{sys}}$, assuming full correlation of the systematic uncertainties. Adding both uncertainties in quadrature results in a deviation from 1 by 1σ . In later fits, tests have been performed rescaling the data so that the error weighted mean of the data points in the first bin is one. The changes observed in the fit results are covered by the errors given.

Data on T [21] are available from MAMI. Our data extend the energy range of the MAMI data. However, the comparison of our T -data and the MAMI T -data reveals serious discrepancies (see Fig. 4). On average, the MAMI T -asymmetry are smaller than our results by a factor 0.7. If an overall scaling factor of 0.7 is introduced, the two data sets agree nicely. The difference $\Delta T = T_{\text{MAMI}}/0.7 - T_{\text{ELSA}}$, normalized to the statistical error, results in a Gaussian distribution centered at zero with a width of $\sigma = 1.09 \pm 0.07$. The origin of this discrepancy is not understood. The same analysis based on the same CBELSA/TAPS-data set was used to derive T for $\gamma p \rightarrow p\pi^0$ [35, 36]. These results and the MAMI results for $T(\gamma p \rightarrow p\pi^0)$ [49] are fully consistent.

T , P , H , and G are small as expected and as predicted by most partial-wave analyses. The data sets are shown in comparison to various PWA-predictions. Already at low energies, below $E_\gamma=1$ GeV ($W=1.660$ GeV), the PWA-predictions show significant deviations from the data, above $E_\gamma=1$ GeV, the data and the predictions diverge: none of the partial-wave analyses predicted all observables with reasonable accuracy. Large deviations from the data are observed for the predictions from SAID [51], BnGa2011 [18], and the JüBo model [32] (JüBo 2015-3, includes the recent CLAS-data on E [22]). MAID2018 [26], which includes recent data on E [22] and T , F [21], exhibits fewer deviations but still fails to predict e.g. G . The comparison shows how important these new data are to constrain the amplitudes for photoproduction of η mesons off protons.

3.2. PWA fits

These data, and further new $\gamma p \rightarrow p\eta$ -data from MAMI $\frac{d\sigma}{d\Omega}$ [20], (T, F) [21], CLAS Σ [52], E [22], and CBELSA/

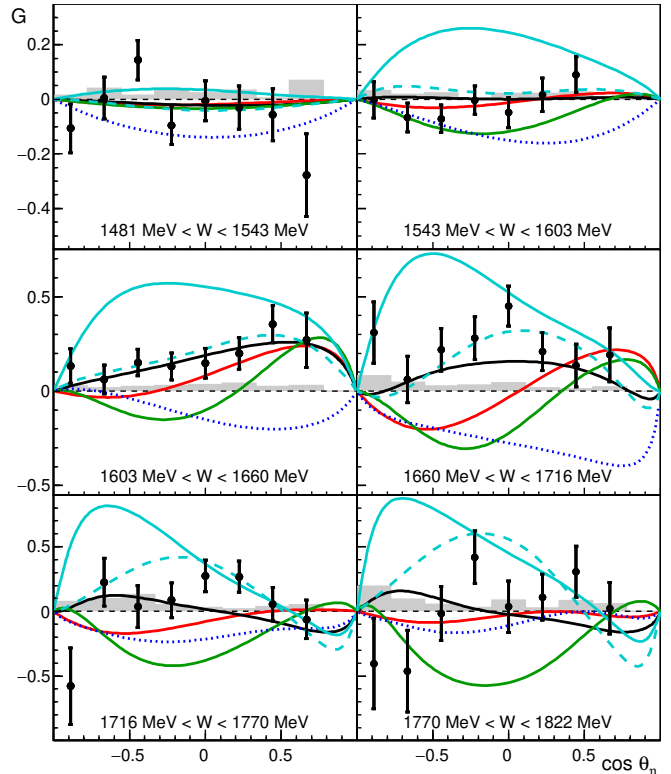


Figure 7: The double polarization observable G as function of $\cos \theta_\eta$, where θ_η is the η production angle in the cms for different cms energy ranges. See caption of Fig. 4 for an explanation of the symbols.

TAPS Σ [61] as well as the η' -data sets used in [62] are included in the data base used in [18]. The full data base also includes the GWU πN partial-wave amplitudes and data on the pion and photo-produced πN , ηN , and KY (Y : hyperon) final states [53, 54, 55]. Also the data on $\pi^- p \rightarrow \eta n$ [56, 57, 58] are included. (For a complete list of data sets included into the BnGa-PWA, see also: [63].) In the study presented here, the couplings to the $\pi^0\pi^0 N$ and $\pi^0\eta p$ final state are frozen to values derived in [59, 60]. For the differential cross sections scaling factors were used in the fit to take care about normalization inconsistencies.

3.3. $N^* \rightarrow N\eta$ decays

Table 1 presents the resonances used in the fit and the resulting branching ratios for $N^* \rightarrow N\eta$ decays. The uncertainties result from a variation of the fit hypothesis, in particular the inclusion of additional resonances or the exclusion of minor resonances in the fit. We studied the effect the systematic difference visible in T between the MAMI (T, F) and the CBELSA/TAPS data (T, P, H) might have on the fit. To do so we allowed either for scaling factors in the MAMI T, F -data or in the CBELSA/TAPS T, P, H -data. When scaling factors for the MAMI-data were admitted, they optimized at 0.73 for T and 0.67 for F resulting in a χ^2/N_{data} for the two data sets of 1.608 and 1.464. These χ^2/N_{data} values are almost identical to the values of the final fit ($\chi^2/N_{\text{data}}=1.609, 1.465$, respectively) where we fixed the scaling factor to 0.7 as determined

experimentally for T . Next, the MAMI T, F -data were included in the fit without scaling factors, while scaling factors were introduced for the CBELSA/TAPS T, P, H -data. The χ^2/N_{data} for the MAMI T, F -data was found to significantly worse ($\chi^2/N_{\text{data}}=3.3, 2.5$, respectively), the χ^2/N_{data} for the CBELSA/TAPS T got slightly worse, it improved slightly for P and remained the same for H . At the same time the overall weighed [18] χ^2/N_{data} of the fit for all $\gamma p \rightarrow p\eta$ -data sets increased from $\chi^2/N_{\text{data}}=1.42$ (final fit) to $\chi^2/N_{\text{data}}=1.5$. Obviously, the fit constrained by the existing $p\eta$ -data sets finds a better consistency between the different data sets when MAMI (T, F)-data were scaled. The variations in the branching ratios (BR) and helicity amplitudes ($A_{1/2}, A_{3/2}$) found in these studies are covered by the errors given in Tab. 1.

There are a few remarkable observations: The $N\eta$ -BR for $N(1535)1/2^-$ is now 0.41 ± 0.04 (instead of the most recent PDG value of $0.42^{+0.13}_{-0.12}$). Since the statistical error is negligible compared to the systematic error, we quote only the latter one. Note that our error includes the uncertainty due to the $N(1535)1/2^-$ helicity amplitude $A_{1/2} = (0.096 \pm 0.008) \text{ GeV}^{-1/2}$. Second, there is a significant change in the $N(1650)1/2^- \rightarrow N\eta$ branching ratio: it changes from 0.05–0.15 (RPP 2014) and 0.14–0.22 (RPP 2017) to 0.33 ± 0.04 in our present fit, reducing substantially the puzzling difference in the magnitude of the $N\eta$ branching ratios of $N(1535)1/2^-$ and $N(1650)1/2^-$. Furthermore, also the $N(1900)3/2^+ \rightarrow N\eta$ branching ratio changed from ≈ 0.12 (RPP 2014) and 0.02–0.14 (RPP 2017) to 0.02 ± 0.02 . The $N(1875)3/2^- \rightarrow N\eta$ branching ratio is now found to be 0.10 ± 0.06 . All other values are well within the earlier error bars; some $N^* \rightarrow N\eta$ branching ratios are new (even though rather small). The $N(1710)1/2^+ \rightarrow N\eta$ branching ratio settles at 0.18 ± 0.10 , well inside its previous range 0.05–0.55, while $N(1720)3/2^+$ contributes very little. These results clearly show the power of polarization observables to constrain PWAs; an earlier PWA [23] not including these indicated a large $N(1720)3/2^+$ contribution.

3.4. The $N(1650)1/2^- \rightarrow N\eta$ branching ratio

The large change in the $N(1650)1/2^- \rightarrow N\eta$ branching ratio deserves a more detailed discussion. Here we restrict ourselves to a discussion of analyses that include data on photoproduction. The data on reaction $\pi^- p \rightarrow \eta n$ are not sufficiently precise to allow for an unambiguous separation of the contributing partial waves.

The BnGa group reported a $N\eta$ branching ratio of $\text{BR}(N\eta) = 0.18 \pm 0.04$ and a helicity coupling of $A_{1/2} = 0.033 \pm 0.007 \text{ GeV}^{-1/2}$ [18]. The helicity coupling and its error were estimated from 12 fits with acceptable χ^2 , which made different assumptions on the number of contributing resonances. Two classes of results were found (BnGa2011-01 and BnGa2011-02). The solution BnGa2011-01 gave a helicity amplitude $A_{1/2} = 0.028 \pm 0.005 \text{ GeV}^{-1/2}$ and a branching ratio $\text{BR}(N\eta) = 0.16 \pm 0.05$, solution BnGa2011-

02 a helicity amplitude $A_{1/2} = 0.038 \pm 0.005 \text{ GeV}^{-1/2}$ and a branching ratio $\text{BR}(N\eta) = 0.21 \pm 0.02$.

With the new data, solutions with two $J^P = 5/2^+$ resonance poles only became significantly worse and fits with this hypothesis were no longer included in the calculation of averages. This leads to an increase of the helicity amplitude and the $N\eta$ branching ratio to $A_{1/2} = 0.036 \pm 0.005 \text{ GeV}^{-1/2}$ and $\text{BR}(N\eta) = 0.22 \pm 0.04$, respectively if only the solutions with 3 poles in BnGa2011-01 and BnGa2011-02 [18] are considered. Based on the fits to the new data, an additional increase of $A_{1/2}\sqrt{\text{BR}(N\eta)}$

Table 1: Branching ratios (BR) for $N^* \rightarrow N\eta$ decays and the photon helicity amplitudes $A_{1/2}, A_{3/2}$ of nucleon resonances, both calculated at their pole positions. The helicity amplitudes are given in units of $\text{GeV}^{-1/2}$. Small numbers below the BRs give the RPP 2017 [30] (representing the status before new η (double) polarization data became available from CLAS, MAMI and CBELSA/TAPS). $A_{1/2}, A_{3/2}$ at the pole positions are complex numbers. Here we give the absolute value with a positive sign if the phase falls between -45° and $+45^\circ$, a negative sign for $135^\circ < \phi < 225^\circ$ and “*” otherwise. The small values below the helicity amplitudes $A_{1/2}, A_{3/2}$ give values from [59], if available, otherwise marked by (R) values from [66] are given, since no PDG-estimates exist for this quantity.

Res.	$\text{BR}(N^* \rightarrow N\eta)$	Res.	$\text{BR}(N^* \rightarrow N\eta)$
$A_{1/2}$	$A_{3/2}$	$A_{1/2}$	$A_{3/2}$
$N(1535)$ $1/2^-$	0.41 ± 0.04 $0.32-0.52$	$N(2120)$ $3/2^-$	≤ 0.01 -
$+0.096 \pm 0.008$ $+0.114 \pm 0.008$	-	$+0.110 \pm 0.045$ $+0.130 \pm 0.045$	$+0.130 \pm 0.050$ $+0.160 \pm 0.060$
$N(1650)$ $1/2^-$	0.33 ± 0.04 $0.14 - 0.22$	$N(1720)$ $3/2^+$	0.03 ± 0.02 $0.01-0.05$
$+0.032 \pm 0.006$ $+0.032 \pm 0.06$	-	$+0.090 \pm 0.035$ $+0.115 \pm 0.045$	$*0.120 \pm 0.035$ $*0.140 \pm 0.040$
$N(1895)$ $1/2^-$	0.10 ± 0.05 $0.15-0.27$	$N(1900)$ $3/2^+$	0.02 ± 0.02 $0.02-0.14$
-0.030 ± 0.010 -0.015 ± 0.006	-	$*0.026 \pm 0.014$ $*0.026 \pm 0.014$	$*0.090 \pm 0.020$ $*0.070 \pm 0.030$
$N(1710)$ $1/2^+$	0.18 ± 0.10 $0.10 - 0.50$	$N(1675)$ $5/2^-$	0.005 ± 0.005 < 0.01
$*0.035 \pm 0.015$ $*0.028^{+0.009}_{-0.002}$ (R)	-	$+0.020 \pm 0.004$ $+0.022 \pm 0.003$	$+0.028 \pm 0.005$ $+0.028 \pm 0.006$
$N(1880)$ $1/2^+$	0.18 ± 0.08 $0.05 - 0.55$	$N(2060)$ $5/2^-$	0.06 ± 0.02 $0.02 - 0.06$
$+0.040 \pm 0.015$ -	-	$+0.070 \pm 0.010$ $+0.064 \pm 0.010$	$+0.070 \pm 0.020$ $+0.060 \pm 0.020$
$N(2100)$ $1/2^+$	0.30 ± 0.15 seen	$N(1680)$ $5/2^+$	0.002 ± 0.001 < 0.01
$*0.010 \pm 0.004$ $*0.011 \pm 0.004$	-	-0.014 ± 0.002 -0.013 ± 0.003	$+0.134 \pm 0.005$ $+0.135 \pm 0.005$
$N(1520)$ $3/2^-$	< 0.001 < 0.01	$N(2000)$ $5/2^+$	0.02 ± 0.02 < 0.04
-0.024 ± 0.004 -0.023 ± 0.004	$+0.128 \pm 0.006$ $+0.131 \pm 0.006$	$+0.015 \pm 0.006$ $+0.033 \pm 0.010$	-0.043 ± 0.008 -0.045 ± 0.008
$N(1700)$ $3/2^-$	0.01 ± 0.01 seen	$N(2190)$ $7/2^-$	0.04 ± 0.02 seen
$*0.045 \pm 0.012$ $*0.047 \pm 0.016$	-0.055 ± 0.012 -0.041 ± 0.014	-0.070 ± 0.020 -0.068 ± 0.005	$+0.039 \pm 0.007$ $+0.025 \pm 0.010$
$N(1875)$ $3/2^-$	0.10 ± 0.06 < 0.01	$N(1990)$ $7/2^+$	0.01 ± 0.01 -
$*0.008 \pm 0.006$ $*0.017 \pm 0.009$	$*0.008 \pm 0.004$ -0.008 ± 0.004	$+0.070 \pm 0.020$ $*0.010^{+0.011}_{-0.006}$ (R)	$+0.044 \pm 0.008$ $+0.053^{+0.023}_{-0.028}$ (R)

by about 9% is observed while the values for $A_{1/2}$ and $\text{BR}(N\eta)$ optimize at $A_{1/2} = 0.032 \pm 0.006 \text{ GeV}^{-1/2}$ and $\text{BR}(N\eta) = 0.33 \pm 0.04$.

The change of the result on the $N\eta$ branching ratio of $N(1650)1/2^-$ is hence due to the facts that one set of solutions is discredited by new data, that $A_{1/2}\sqrt{\text{BR}(N\eta)}$ is slightly increased and that the fit optimizes at a slightly lower helicity coupling.

In 2012, Shklyar *et al.* [17] published the results of a coupled-channel analysis of a large number of reactions (of course not yet including the new observables becoming available only recently). The authors gave a branching ratio of 0.01 ± 0.02 , which we read as < 0.03 and used a helicity coupling of 0.063 ± 0.007 . If our value on $A_{1/2}$ is used, the upper limit increases to < 0.12 . It is still incompatible with our finding but the discrepancy is reduced. Similar arguments hold true for the results presented in [15, 16].

The value for $A_{1/2}\sqrt{\text{BR}(N\eta)}$ found by $\eta\text{MAID}2017$ [20] and $\text{MAID}2018$ [26] is consistent with our findings.

With our value for $A_{1/2}$, the $N\eta$ branching ratio above 1 would be determined from the results presented by Tryaschev [28]. In [28] a high intensity is assigned to $N(1720)3/2^+$ and the fit quality is not absolutely convincing. Thus we do not believe that this result excludes the branching ratio reported in this letter.

Interesting results can be expected if the data presented here will be included in other analyses as planned, e.g., within the JüBo coupled-channel analysis [67].

4. Summary

Summarizing, we have determined the polarization observables E, T, H, P , and G for the reaction $\gamma p \rightarrow \eta p$ from measurements using a polarized beam and a polarized target. Further, the new measurements on the differential cross section $d\sigma/d\Omega$ [20], and new data on the beam asymmetry Σ [52, 61], on the polarization observables T, F [21] from MAMI, and on E from CLAS [22] were added to the data base [18]. The new data provide significant new constraints on the η -photoproduction amplitude. Branching ratios for $N^* \rightarrow N\eta$ decays were determined. The large $N(1650)1/2^- \rightarrow N\eta$ branching ratio found is surprising, given the previously large difference in the $N\eta$ branching ratios of the $N(1535)1/2^- / N(1650)1/2^-$ nucleon-resonance pair, which was extensively discussed in literature (see [64] for a summary and the examples in the introduction). In the standard quark model, this has been taken as evidence for a large mixing of $\text{SU}(6) \times \text{O}(3)$ states (see Review on Quark Models in [31]). Together with the inversion of the relative sign of the electromagnetic couplings of the $N(1535)1/2^-$ and the $N(1650)1/2^-$ state for photoproduction off the proton and the neutron [65], the interpretation of these states within the quark model will have to be revised.

We thank the technical staff of ELSA and the participating institutions for their invaluable contributions to

the success of the experiment. We acknowledge support from the *Deutsche Forschungsgemeinschaft* (SFB/TR16 and SFB/TR110), the *U.S. Department of Energy, Office of Science, Office of Nuclear Physics under Awards No. DE-FG02-92ER40735*, the *Russian Science foundation*, and the *Schweizerischer Nationalfonds (200020-156983, 132799, 121781, 117601)*.

References

- [1] N. Isgur and G. Karl, Phys. Lett. B **72**, 109 (1977).
- [2] S. Capstick and N. Isgur, Phys. Rev. D **34**, 2809 (1986).
- [3] L. Y. Glozman, D. O. Riska, Phys. Rept. **268**, 263 (1996).
- [4] U. Löring *et al.*, Eur. Phys. J. A **10**, 395 (2001).
- [5] R. G. Edwards *et al.*, Phys. Rev. D **84**, 074508 (2011).
- [6] J. C. Nacher *et al.*, Nucl. Phys. A **678**, 187 (2000).
- [7] E. E. Kolomeitsev *et al.*, Phys. Lett. B **585**, 243 (2004).
- [8] P. C. Bruns, M. Mai and U. G. Meissner, Phys. Lett. B **697**, 254 (2011)
- [9] M. Mai, P. C. Bruns and U.-G. Meissner, Phys. Rev. D **86**, 094033 (2012).
- [10] K. Nakamura *et al.* (PDG), JPG **37**, 075021 (2010).
- [11] L. Y. Glozman, D. O. Riska, Phys. Lett. B **366**, 305 (1996).
- [12] B. S. Zou, Eur. Phys. J. A **35**, 325 (2008).
- [13] N. Kaiser *et al.*, Phys. Lett. B **362**, 23 (1995).
- [14] T. P. Vrana, S. A. Dytman, and T. S. H. Lee, Phys. Rept. **328**, 181 (2000).
- [15] G. Penner and U. Mosel, Phys. Rev. C **66**, 055211 (2002).
- [16] G. Penner and U. Mosel, Phys. Rev. C **66**, 055212 (2002).
- [17] V. Shklyar H. Lenske, and U. Mosel, Phys. Rev. C **87**, 015201 (2013).
- [18] A. V. Anisovich *et al.*, Eur. Phys. J. A **48**, 15 (2012).
- [19] U. Thoma *et al.*, Phys. Lett. B **659**, 87 (2008).
- [20] V. L. Kashevarov *et al.* [A2 Collaboration], Phys. Rev. Lett. **118**, no. 21, 212001 (2017).
- [21] C. S. Akondi *et al.*, Phys. Rev. Lett. **113**, 102001 (2014).
- [22] I. Senderovich *et al.*, Phys. Lett. B **775**, 64 (2016).
- [23] V. Crede *et al.*, Phys. Rev. Lett. **94** 012004 (2005), Phys. Rev. C **80**, 055202 (2009).
- [24] O. Bartalini *et al.* [GRAAL Collaboration], Eur. Phys. J. A **33**, 169 (2007)
- [25] M. Williams *et al.* [CLAS Collaboration], Phys. Rev. C **80**, 045213 (2009)
- [26] L. Tiator *et al.*, Eur. Phys. J. A **54**, no. 54, 210 (2018).
- [27] M. Shrestha and D. M. Manley, Phys. Rev. C **86**, 055203 (2012).
- [28] V. A. Tryaschev, Eur. Phys. J. A **50**, 120 (2014).
- [29] K. A. Olive *et al.*, Chin. Phys. C **38**, 090001 (2014).
- [30] C. Patrignani *et al.* (Particle Data Group), Chin. Phys. C, **40**, 100001 (2016) and 2017 update.
- [31] M. Tanabashi *et al.* (Particle Data Group), Phys. Rev. D **98**, 030001 (2018) and 2019 update.
- [32] D. Rönchen *et al.*, Eur. Phys. J. A **51** 70 (2015).
- [33] M. Gottschall *et al.*, Phys. Rev. Lett. **112**, 012003 (2014).
- [34] M. Gottschall *et al.* [CBELSA/TAPS Collaboration], arXiv:1904.12560 [nucl-ex].
- [35] J. Hartmann *et al.*, Phys. Rev. Lett. **113**, 062001 (2014).
- [36] J. Hartmann *et al.* [CBELSA/TAPS Collaboration], Phys. Lett. B **748**, 212 (2015)
- [37] A. Thiel *et al.*, Phys. Rev. Lett. **109**, 102001 (2012).
- [38] A. Thiel *et al.*, arXiv:1604.02922 [nucl-ex] (2016).
- [39] W. Hillert, Eur. Phys. J. A **28S1**, 139 (2006).
- [40] H. Dutz, Nucl. Instrum. Meth. A **526**, 117 (2004).
- [41] G. Suft *et al.*, Nucl. Instrum. Meth. A **538**, 416 (2005).
- [42] E. Aker *et al.*, Nucl. Instrum. Meth. A **321**, 69 (1992).
- [43] R. Novotny, IEEE Trans. Nucl. Sci. **38**, 379 (1991).
- [44] T. Seifen, J. Hartmann *et al.*, in preparation.
- [45] H. Olsen and L. C. Maximon, Phys. Rev. **114**, 887 (1959).
- [46] D. Elsner *et al.*, Eur. Phys. J. A **39**, 373 (2009).
- [47] F.A. Natter *et al.*, Nucl. Instrum. Meth. B **221**, 465 (2004).

- [48] G. Reicherz *et al.*, Nucl. Instrum. Meth. A **356**, 74 (1995).
- [49] J. R. M. Annand *et al.* [A2 and MAMI Collaborations], Phys. Rev. C **93**, no. 5, 055209 (2016). doi:10.1103/PhysRevC.93.055209
- [50] D. Drechsel *et al.*, Eur. Phys. J. A **34**, 69 (2007).
- [51] SAID: <http://gwdac.phys.gwu.edu/>
- [52] P. Collins *et al.*, Phys. Lett. B **771**, 213 (2017)
- [53] A. Anisovich *et al.*, Eur. Phys. J. A **24**, 111 (2005).
- [54] A. V. Anisovich and A. V. Sarantsev, Eur. Phys. J. A **30**, 427 (2006).
- [55] A. V. Anisovich *et al.*, Eur. Phys. J. A **34**, 129 (2007).
- [56] W. B. Richards *et al.*, Phys. Rev. D **1**, 10 (1970).
- [57] R. M. Brown *et al.*, Nucl. Phys. B **153**, 89 (1979).
- [58] S. Prakhov *et al.*, Phys. Rev. C **72**, 015203 (2005).
- [59] V. Sokhoyan *et al.*, Eur. Phys. J. A **51**, no. 8, 95 (2015), [Eur. Phys. J. A **51**, no. 12, 187 (2015)].
- [60] E. Gutz *et al.* Eur. Phys. J. A **50** 74 (2014).
- [61] F. Afzal *et al.* [CBELSA/TAPS Collaboration], “Precise beam asymmetry Σ data for $\gamma p \rightarrow p\eta$ in the $p\eta'$ -threshold region”, in preparation
- [62] A. V. Anisovich *et al.*, Phys. Lett. B **772**, 247 (2017).
- [63] <https://pwa.hiskp.uni-bonn.de/>
- [64] B. Krusche *et al.*, Prog. Part. Nucl. Phys. **51**, 399 (2003).
- [65] A. V. Anisovich *et al.*, Eur. Phys. J. A **51**, no. 6, 72 (2015).
- [66] D. Rönchen *et al.*, Eur. Phys. J. A **50**, no. 6, 101 (2014) Erratum: [Eur. Phys. J. A **51**, no. 5, 63 (2015)]
- [67] D. Rönchen, private communication